


Unveiling Temperature-Dependence Mechanisms of Perpendicular Magnetic Anisotropy at Fe/MgO Interfaces

Fatima Ibrahim^{1,*}, Ali Hallal¹, Alan Kalitsov,² Derek Stewart,² Bernard Dieny,¹ and Mairbek Chshiev^{1,3,†}

¹*Université Grenoble Alpes, CEA, CNRS, SPINTEC, Grenoble 38000, France*

²*Western Digital Technologies, Inc., 5601 Great Oaks Parkway, San Jose, California 95119, USA*

³*Institut Universitaire de France (IUF), 75231 Paris, France*

 (Received 11 March 2021; revised 3 March 2022; accepted 18 April 2022; published 25 May 2022)

The perpendicular magnetic anisotropy at magnetic transition-metal–oxide interfaces is a key element in building out-of-plane magnetized magnetic tunnel junctions for spin-transfer-torque magnetic random access memory (STT MRAM). Size downscaling renders magnetic properties more sensitive to thermal effects. Thus, understanding the temperature dependence of the magnetic anisotropy becomes crucial. In this work, we theoretically address the correlation between the temperature dependence of magnetic anisotropy and magnetization in typical Fe/MgO-based structures. In particular, the possible mechanisms behind the experimentally reported deviations from the Callen and Callen scaling power law are analyzed. At ideal interfaces, first-principles calculations reveal (i) small high-order anisotropy constants compared to first order and (ii) enhanced exchange constants. Considering these two intrinsic effects in the atomistic simulations, the temperature-dependence of the total and layer-resolved anisotropy are found to follow the Callen and Callen scaling power law, thus ruling out an intrinsic microscopic mechanism underlying deviations from this law. Besides, two possible extrinsic macroscopic mechanisms are unveiled, namely the influence of the dead layer, often present in the storage layer of STT-MRAM cells and the spatial inhomogeneities of the interfacial magnetic anisotropy. About the first mechanism, we show that the presence of a dead layer tends to reduce the scaling exponents. In the second mechanism, increasing the percentage of inhomogeneity in the interfacial perpendicular magnetic anisotropy is revealed to decrease the scaling exponent. These results allow us to coherently explain the difference in scaling exponents relating anisotropy and magnetization thermal variations reported in earlier experiments. This is crucial for the understanding of the thermal stability of the storage-layer magnetization in STT-MRAM applications.

DOI: [10.1103/PhysRevApplied.17.054041](https://doi.org/10.1103/PhysRevApplied.17.054041)

I. INTRODUCTION

The evolution in magnetic random access memory (MRAM) technologies has been made possible due to fundamental research breakthroughs in spintronic phenomena and materials development. Intensive efforts have been focused on spin transfer torque (STT) [1,2], which enables current-induced switching and thus better down-scalability compared to field-written MRAM [3–6]. More precisely, perpendicular STT MRAMs where out-of-plane magnetized magnetic tunnel junctions serve as storage elements provide both low switching currents, owing to the relatively weak Gilbert damping, and high thermal stability due to their large perpendicular magnetic anisotropy (PMA) values [7–9]. PMA has been observed to be common at magnetic metal–oxide interfaces with

either amorphous or crystalline oxides [10–12] and has been theoretically attributed to the electronic hybridization between the oxygen and magnetic transition-metal orbitals across the interface [13].

The memory retention, which is determined by the thermal stability of the storage-layer magnetization, is directly related to the PMA of this layer. This is a key parameter in STT-MRAM applications. The concept of thermally assisted STT MRAM has also been proposed to reduce the write current while maintaining a large thermal stability factor [14]. With regard to applications, the sensitivity of magnetic properties to temperature is a critical point, especially for applications that have to operate over a broad range of temperatures, such as automotive applications. This emphasizes the need for a fundamental understanding of the PMA dependence on temperature. In this context, the correlation between the temperature-dependent anisotropy constant K and the magnetization M of ferromagnets, as described by Callen

*fatima.ali.ibrahim@hotmail.com

†mair.chshiev@cea.fr

and Callen, follows a power scaling law: $K(T)/K(0) = [M(T)/M(0)]^n$, with $n = i(2i + 1)$ corresponding to the i th-order anisotropy constant [15,16]. It follows that for the first-order anisotropy constant K_1 , a scaling exponent $n = 3$ is expected. However, deviations from this law with scaling exponents $n < 3$ have been experimentally reported [17–19]. This has been explained by the two-ion anisotropy model in $L1_0$ Fe-Pt alloys [20,21] and more recently in (Co-Fe-B)/MgO structures [19]. However, considering various mechanisms that are likely to occur in actual devices and their probable contribution to the temperature dependence of the magnetic properties, the analysis of the relationship between thermal variations of anisotropy and magnetization requires further clarification. For instance, the effect of a magnetic dead layer, which often forms when using buffer or capping layers for transition-metal–oxide structures [22], has not been addressed so far. Since the thickness of the dead layer is temperature dependent, considering its effect on the correlation between the temperature dependencies of K and M becomes essential. Another possible effect is the spatial thickness fluctuations at the interface [23], which give rise to a second-order anisotropy, K_2 , contribution manifested as canted or easy-cone magnetic states [24]. All this emphasizes the importance of clarifying the mechanisms contributing to the temperature dependence of magnetic anisotropy and whether they are micro- or macroscopic in nature. In particular, the mechanisms underlying deviations from the theoretical Callen and Callen power law require further investigation.

In this paper, we study theoretically the correlation between the temperature dependencies of magnetic anisotropy and magnetization in typical Fe/MgO-based structures, addressing several fundamental and practical aspects. Our first-principles calculations carried out on ideal structure reveal that the second-order magnetic anisotropy constant K_2 is one order of magnitude smaller than its first-order one, K_1 , indicating that higher-order anisotropy terms of intrinsic magnetocrystalline origin are unlikely to account for temperature-dependent mechanisms. Neglecting higher-order anisotropy contributions to the atomistic spin Hamiltonian, calculations are performed in order to unveil the macroscopic mechanisms of the temperature dependence of magnetic anisotropy. After calculating the layer-resolved exchange constants in an ideal Fe/MgO interface, we demonstrate that inclusion of the effect of enhanced exchange at the interface is crucial to obtain scaling exponents consistent with the Callen and Callen scaling power law. We elucidate that the layer-resolved temperature dependence of magnetic anisotropy also follows the law, with $n = 3$. Next, two mechanisms that are very likely to occur in magnetic metal–oxide structures are considered and their impact on the correlation between the temperature dependencies of K and M is analyzed. It is shown that the presence of a magnetic

dead layer yields lower effective scaling exponents that deviate from the theoretical law. The second mechanism reveals that increasing the percentage of inhomogeneity in the interfacial PMA decreases the scaling exponent. The present results elucidate that the mechanisms behind the deviations from the theoretical Callen and Callen power law are extrinsic (the presence of a dead layer and of interfacial roughness) rather than intrinsic. These results allow us to coherently explain the difference in scaling exponents relating anisotropy and magnetization thermal variations reported in earlier experiments.

The paper is organized as follows. In Sec. II, we present the first-principles calculation results of the first- and second-order anisotropy constants at Fe/MgO interfaces with different terminations. The layer-resolved exchange constants are identified in Sec. III. Then, the atomistic calculations of the temperature dependence of the magnetic anisotropy are presented and discussed in Sec. IV. The effect of a magnetic dead layer is addressed in Sec. V, while Sec. VI is dedicated to the effect of the inhomogeneity in the perpendicular magnetic anisotropy on the temperature dependence. The main conclusions drawn from this study are summed up in Sec. VII.

II. K_1 AND K_2 EVALUATION FROM FIRST PRINCIPLES

The interfacial magnetic anisotropy energy E_{MCA} is obtained from the dependence of the total energy E on the angle θ between the magnetization direction and the normal to the interface, expressed as

$$E_{MCA}(\theta) = E(\theta) - E(0) = K_1 \sin^2 \theta + K_2 \sin^4 \theta + K_3 \sin^6 \theta + \dots = \sum K_i \sin^{2i} \theta. \quad (1)$$

Typically, the first-order term K_1 dominates the higher-order ones in structures with interfacial anisotropy. However, in experiments, the influence of the second-order K_2 has been observed, namely in the formation of an easy-cone state [24,25]. The origin of significant K_2 values is attributed to spatial fluctuations of the film thickness [23,26], strongly interface-concentrated PMA combined with a moderate exchange coupling of the interface moment to the rest of the film [27], or strong magnetic inhomogeneities [28]. Although the aforementioned experiments have been explained by such extrinsic mechanisms, it is necessary to elucidate whether the higher-order anisotropy terms may also be of intrinsic origin. For this, we perform systematic first-principles calculations to quantify the higher-order anisotropy terms in MgO-based interfaces, including Fe/MgO and (Fe-Co)/MgO with either Co or Fe-Co termination. Details of the computation method are provided in Appendix A.

The total energies from first-principles calculations are fitted with Eq. (1) up to the third order. As an example,

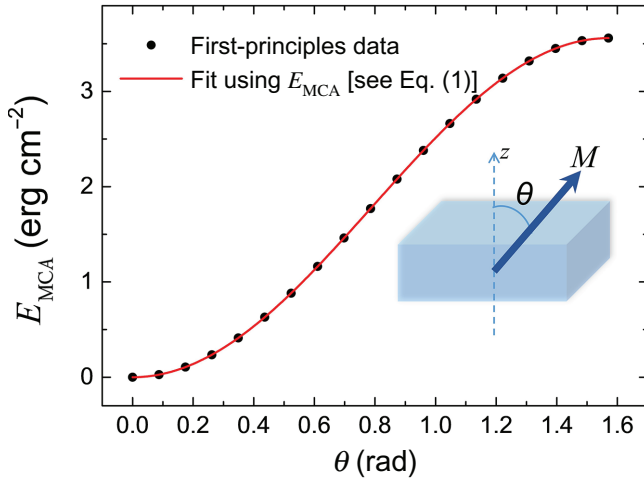


FIG. 1. The magnetic anisotropy energy as a function of the angle θ between the magnetization direction and the normal to the interface calculated for the Fe/MgO structure by first principles (data points), fitted to E_{MCA} [see Eq. (1)] (solid line).

in Fig. 1 we show the result for the case of the Fe/MgO structure. The obtained K_1 and K_2 values for the studied interfaces are summarized in Table I. One can observe that (i) both K_1 and K_2 values are dependent on the interface termination, while (ii) K_2 is found to be one order of magnitude smaller than K_1 and (iii) the K_3 values are found to be negligible for all cases.

To gain more insight, in Fig. 2 we present the layer-resolved K_1 and K_2 values for the different interfaces studied. In the case of Fe/MgO, K_1 is not entirely localized

TABLE I. The first-order K_1 and second-order K_2 anisotropy constants obtained for Fe/MgO and (Fe-Co)/MgO structures with either Co- or Fe-Co-terminated interfaces by fitting the first-principles-calculated E_{MCA} to Eq. (1).

Termination	Fe/MgO Fe	(Fe-Co)/MgO Co	(Fe-Co)/MgO Fe-Co
K_1 (erg cm $^{-2}$)	3.52	0.45	0.87
K_2 (erg cm $^{-2}$)	0.038	0.077	0

at the interface but, rather, propagates into the bulk, showing an attenuating oscillatory behavior [29]. The layer-resolved K_2 for this structure follows K_1 in trend and sign. The situation is different in the case of the (Fe-Co)/MgO interface, showing that for all terminations, K_1 is overall lower compared to that at Fe/MgO and that the PMA originates from the first layer. As for K_2 , it is positive and one order of magnitude smaller than K_1 for the Co-terminated interface, while it is negligible and depends strongly on the atomic distribution for the Fe-Co-terminated interface. Note that the asymmetry in the structure between the two interfaces in the Fe-Co-terminated case is at the origin of the observed asymmetry in the K_2 values [cf. Appendix A(1)].

Based on these findings, we conclude that significant K_2 are not of intrinsic origin in MgO-based interfaces and that their emergence should be attributed to extrinsic mechanisms. In particular, fluctuations of interfacial PMA have been pointed out by experiments [28] and modeled analytically [26] or by micromagnetic simulations [30], giving rise to significant K_2 values. Thus, in order to address

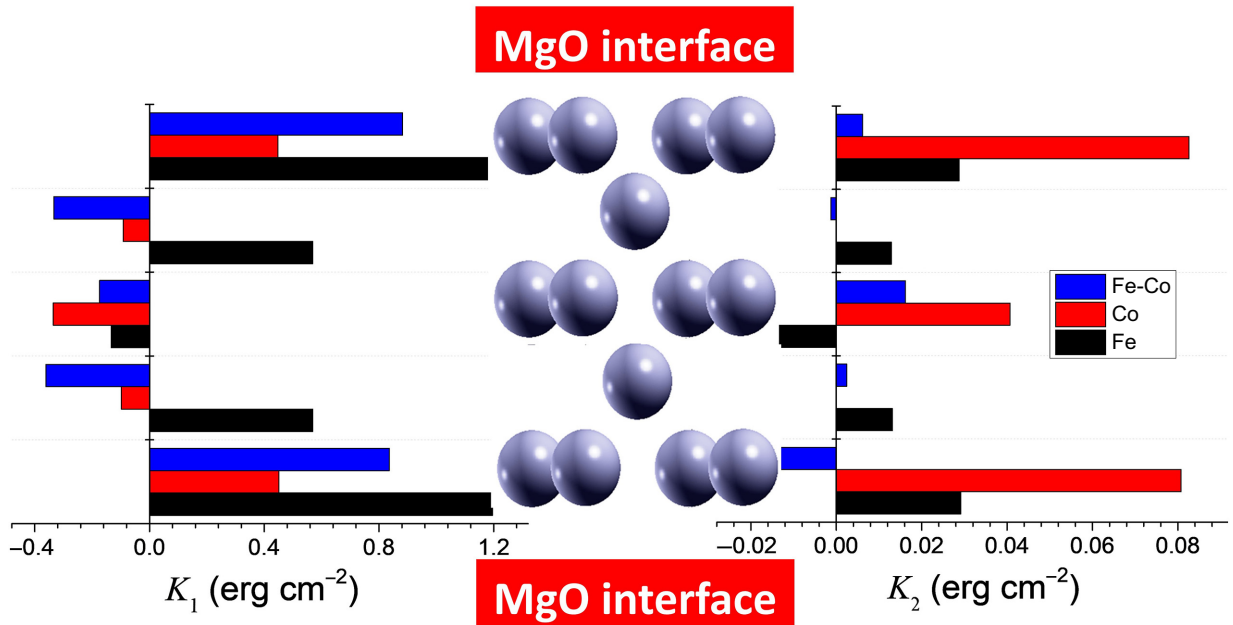


FIG. 2. Layer-resolved values of K_1 and K_2 , obtained from first-principles calculations, compared for Fe/MgO and (Fe-Co)/MgO structures with either Co- or Fe-Co-terminated interfaces.

the temperature dependence of magnetic anisotropy, we exclude K_2 from the atomistic spin Hamiltonian. In the following, we focus instead on exploring two extrinsic mechanisms that are commonly encountered in experiments, namely the presence of a magnetic dead layer and of spatial inhomogeneities in the interfacial PMA.

III. CALCULATION OF THE EXCHANGE CONSTANTS

To study the temperature dependence of magnetic anisotropy, it is important to determine the fundamental parameters that are decisive for this effect. As presented in Appendix A, the first-principles calculations provide both the layer-resolved magnetic moments and anisotropy values at zero temperature. Notably, we observe the enhancement of those two parameters at the two Fe interfacial layers compared to their bulk counterparts, in agreement with previous reports [13,29]. As for the exchange constants, one might expect reduced values at surfaces or interfaces due to the reduced atomic coordination based on a classical Heisenberg model. However, an enhancement of the exchange interaction has been reported at different magnetic surfaces using *ab initio* calculations [31]. Thus, obtaining layer-resolved exchange constants is important not only for characterizing the Fe/MgO interface but also to study macroscopic effects such as magnetic dead layers created by atomic interdiffusion at the Fe/Ta interface, as discussed later.

Using first-principles calculations, we calculate the long-ranged exchange constants in MgO/Fe(*t*)/MgO structures with variable Fe thickness, $5 \leq t$ (ML) ≤ 15 . Since the exchange interaction is strongly distance dependent, truncating it to include only nearest-neighbor interactions

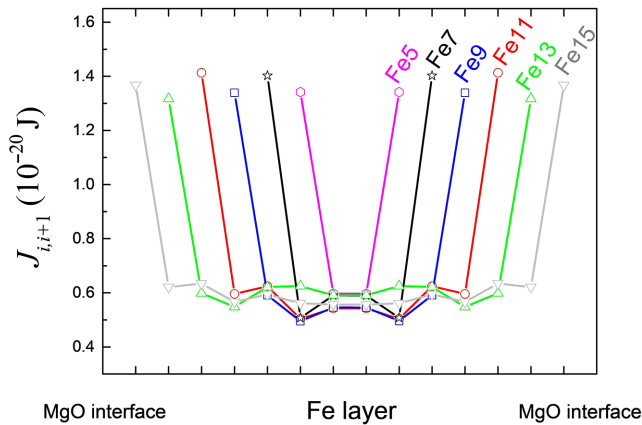


FIG. 3. The layer-resolved nearest-neighbor-exchange constants $J_{i,i+1}$ corresponding to the interaction between atoms in layers i and $i+1$ calculated from first principles in MgO/Fe(*t*)/MgO structures, with the Fe thickness varied between $5 \leq t \leq 15$ monolayers (MLs).

remains a good approximation when used in parametrizing atomistic simulations so as to reduce the computational effort. As explained in Appendix A, this is done by including the tail of the long-ranged exchange into the nearest-neighbor one so that the exchange interaction between atomic monolayers (MLs) remains the same. The layer-resolved nearest-neighbor-exchange pairs $J_{i,i+1}$ between an atom located at layer i and another at $i+1$ are shown in Fig. 3 for a variable Fe thickness. It can be clearly seen that the values of the exchange interaction at the interface [$J_{i,i+1} \approx (1.3 - 1.4) \times 10^{-20}$ J] are well enhanced compared to their bulk-counterpart values [$J_{i,i+1} \approx (5 - 6) \times 10^{-21}$ J], independent of the Fe thickness. This finding is consistent with enhanced exchange interaction reported at the Fe(001) surface [31]. We also note that the presence of quantum-well states leads to the observed oscillations in the bulk exchange values as a function of the distance from the interface [32].

IV. TOTAL AND LAYER-RESOLVED TEMPERATURE DEPENDENCE OF MAGNETIC ANISOTROPY IN IDEAL Fe/MgO INTERFACE

Before investigating the macroscopic mechanisms that contribute to the temperature dependence of magnetic anisotropy, let us first address its total and layer-resolved behavior for an ideal Fe/MgO interface. The details of the calculations are provided in Appendix A(2). We start with a simple model using uniform exchange fixed to the Fe bulk exchange constant ($J = 7 \times 10^{-21}$ J [33]). The 15-ML-thick system comprises one Fe layer with interfacial magnetic anisotropy (Fe1) and the bulk region with negligible anisotropy [Fig. 4(a)]. The normalized saturation magnetization M_s of Fe1 decreases more rapidly with temperature compared to that of the bulk, as shown in Fig. 4(b), due to the reduced atomic coordination at the interface. Next, we fit and compare the calculated anisotropy $K(T)$ to $M_s(T)$ in two cases. If the total saturation magnetization $M_{\text{total}}(T)$ is considered, we obtain a scaling exponent $n = 4.9$ [Fig. 4(c)]. However, use of the interface saturation magnetization $M_{\text{Fe1}}(T)$ yields $n = 3$, i.e., $K_{\text{Fe1}}(T)/K_{\text{Fe1}}(10 \text{ K}) = [M_{\text{Fe1}}(T)/M_{\text{Fe1}}(10 \text{ K})]^3$ following the Callen and Callen law exactly [Fig. 4(d)].

Next, we improve the model by including the layer-resolved exchange constants calculated from first principles while keeping the magnetic anisotropy associated with Fe1 only. In this case, by fitting $K(T)$ to $M_{\text{total}}(T)$, a scaling exponent $n = 3$ is obtained. This emphasizes the importance of including the enhanced interfacial exchange in the model to obtain reasonable scaling exponents. We further improve our model, by including the layer-resolved magnetic anisotropy of the two interfacial Fe layers Fe1 and Fe2. In Fig. 5(a), we compare the layer-resolved saturation magnetization for the three different regions. The magnetization of Fe2 reduces with temperature more slowly than

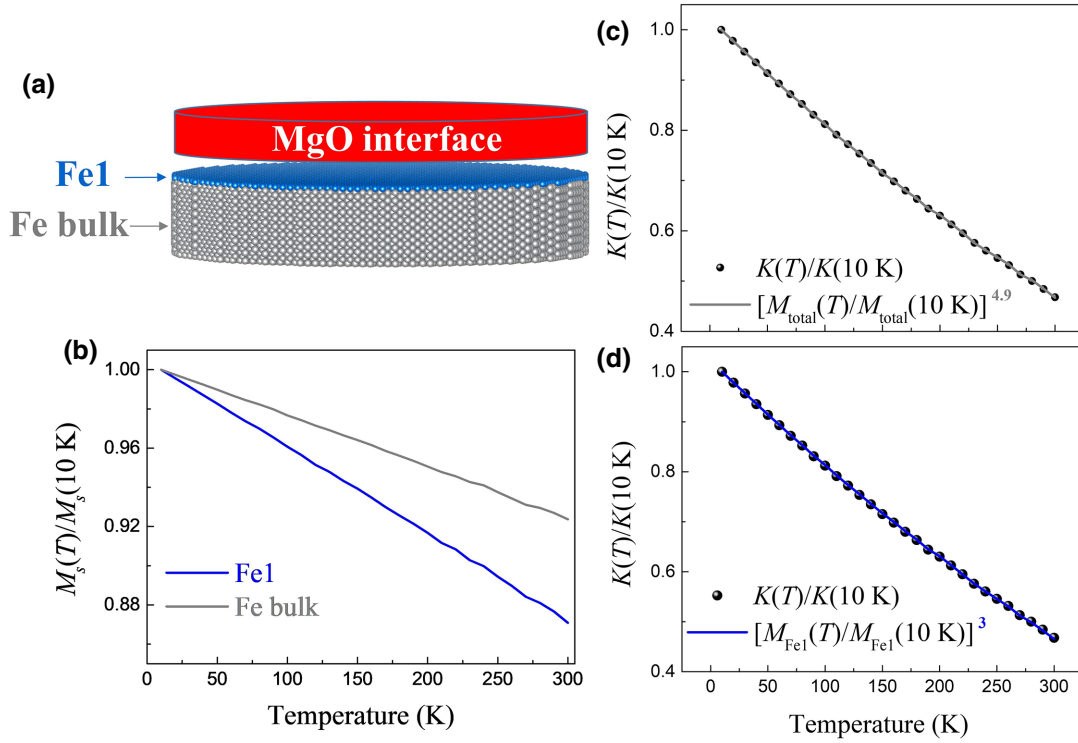


FIG. 4. (a) The model Fe/MgO structure used to calculate the temperature-dependent magnetic properties comprising a bulk Fe region and one interfacial layer (Fe1). (b) The normalized saturation magnetization M_s per region, plotted as a function of temperature. The normalized magnetic anisotropy K as a function of temperature, shown with its fit to the normalized saturation magnetization of the whole structure, M_{total} (resp. the normalized saturation magnetization of the interfacial Fe1 layer M_{Fe1}), yielding scaling exponent $n = 4.9$ (resp. $n = 3$), shown in panel (c) [resp. panel (d)].

that of Fe1 and the bulk region. This can be explained by the enhanced exchange at the interface, namely in the $J_{1,2}$ nearest-neighbor pair interaction, compared to the bulk values, accompanied by a reduced atomic coordination of the Fe1 layer and a full coordination of Fe2. This has a direct implication on the scaling exponent, which is found to be $n = 2.8$ by fitting $K(T)$ to $M_{\text{total}}(T)$.

To extract the per-layer-resolved correlation between $K(T)$ and $M_s(T)$, the results of the previous two models are used. Considering two interfacial Fe MLs, the expression for the temperature-dependent anisotropy can be expanded as

$$\begin{aligned} \frac{K_{\text{Fe1+Fe2}}(T)}{K_{\text{Fe1+Fe2}}(10\text{ K})} &= \frac{K_{\text{Fe1}}(T)}{K_{\text{Fe1}}(10\text{ K})} \left[\frac{K_{\text{Fe1}}(10\text{ K})}{K_{\text{Fe1}}(10\text{ K}) + K_{\text{Fe2}}(10\text{ K})} \right] \\ &+ \frac{K_{\text{Fe2}}(T)}{K_{\text{Fe2}}(10\text{ K})} \left[\frac{K_{\text{Fe2}}(10\text{ K})}{K_{\text{Fe1}}(10\text{ K}) + K_{\text{Fe2}}(10\text{ K})} \right]. \end{aligned} \quad (2)$$

Assuming that the magnetic anisotropy of every Fe layer i ($K_{\text{Fe}i}$) scales as $n = 3$ with its saturation magnetization $M_{\text{Fe}i}$ according to the Callen and Callen power law, Eq. (2)

can be rewritten as

$$\begin{aligned} \frac{K_{\text{Fe1+Fe2}}(T)}{K_{\text{Fe1+Fe2}}(10\text{ K})} &= \left[\frac{M_{\text{Fe1}}(T)}{M_{\text{Fe1}}(10\text{ K})} \right]^3 \left[\frac{K_{\text{Fe1}}(10\text{ K})}{K_{\text{Fe1}}(10\text{ K}) + K_{\text{Fe2}}(10\text{ K})} \right] \\ &+ \left[\frac{M_{\text{Fe2}}(T)}{M_{\text{Fe2}}(10\text{ K})} \right]^3 \left[\frac{K_{\text{Fe2}}(10\text{ K})}{K_{\text{Fe1}}(10\text{ K}) + K_{\text{Fe2}}(10\text{ K})} \right]. \end{aligned} \quad (3)$$

The calculated data accounting for the anisotropy of both Fe1 and Fe2 that yields $n = 2.8$ are then compared to those obtained using Eq. (3) [Fig. 5(b)]. The excellent agreement between the two curves confirms the validity of our assumption that the layer-resolved behavior follows the Callen and Callen scaling power law for each individual Fe layer: $K_{\text{Fe}i}(T)/K_{\text{Fe}i}(10\text{ K}) = [M_{\text{Fe}i}(T)/M_{\text{Fe}i}(10\text{ K})]^3$.

To examine the effect of the sample thickness on the scaling exponent, we use our previously calculated layer-resolved exchange constants for the Fe thickness varying as $5 \leq t \leq 15$ MLs. The scaling exponents obtained by fitting $K(T)$ to $M_{\text{total}}(T)$ as a function of the Fe thickness are shown in Fig. 6 and lie in the range $2.8 \leq n \leq 3.1$. This demonstrates that the Callen and Callen power law holds

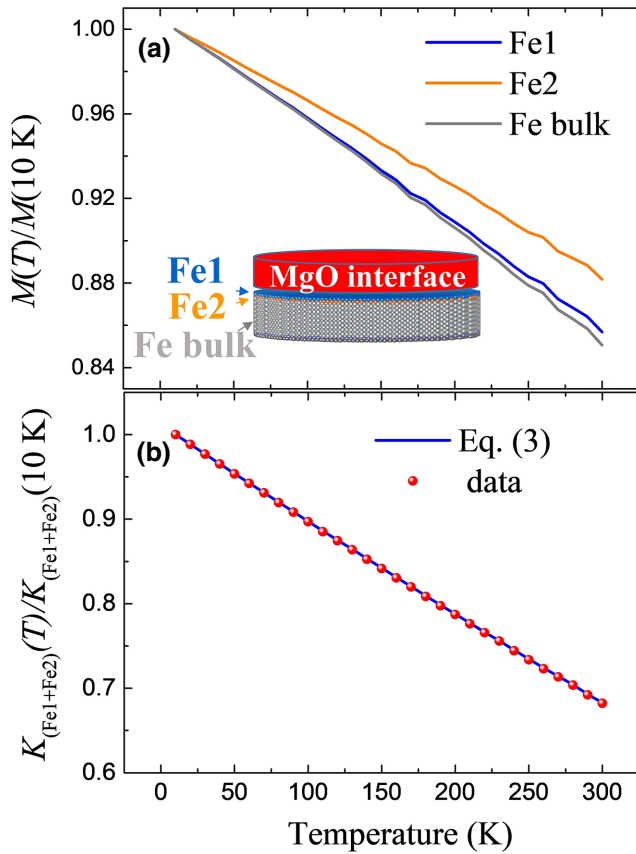


FIG. 5. (a) The normalized saturation magnetization M_s per region as a function of temperature for the model Fe/MgO structure used to calculate the temperature-dependent magnetic properties, comprising a bulk Fe region and two interfacial layers (Fe1 and Fe2). (b) The calculated normalized magnetic anisotropy $K_{\text{Fe1+Fe2}}$ as a function of temperature, shown by circle data points. The solid line corresponds to Eq. (3).

for the anisotropy of Fe/MgO interfaces independent of the sample thickness. This is remarkable, given that the enhanced exchange at the interface is crucial to obtain reasonable values of the scaling exponent around 3. Based on all this, one can conclude that an ideal Fe/MgO interface with its intrinsic properties cannot explain the observed deviations from the Callen and Callen power law. This finding indicates that the deviations may be due to macroscopic effects, which we address in the remainder of this paper.

V. EFFECT OF MAGNETIC DEAD LAYER

Magnetic dead layers form when the atoms of the capping or buffer layer diffuse into the magnetic region upon annealing, resulting in reduced coordination. We therefore choose to model the dead layer by introducing Ta diffusion in the outermost four Fe layers opposite to the Fe/MgO interface, with respective Ta percentages of 100, 75, 50, and 25% (see the inset of Fig. 7) [34]. After relaxing the

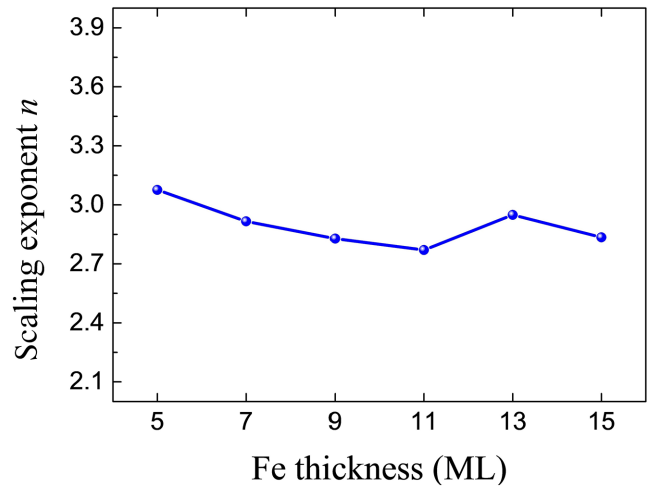


FIG. 6. The scaling exponent n of the temperature dependence of the magnetic anisotropy for an Fe/MgO interface, calculated as a function of the Fe thickness.

structure, the nearest-neighbor-exchange constants are calculated and are compared to those of an ideal Fe/MgO interface in Fig. 7. Using those exchange constants, atomistic calculations for variable system thickness are performed in order to extract the dead-layer thickness. We find that the estimated dead-layer thickness t_{dead} is negligible at sufficiently low temperatures [region (i) in Fig. 8], since the Fe layers hosting Ta atoms still contribute a substantial saturation magnetization M_s (see Appendix C). However, increasing the temperature results in the decrease of their M_s values, which in turn increases the dead-layer thickness [region (ii) in Fig. 8].

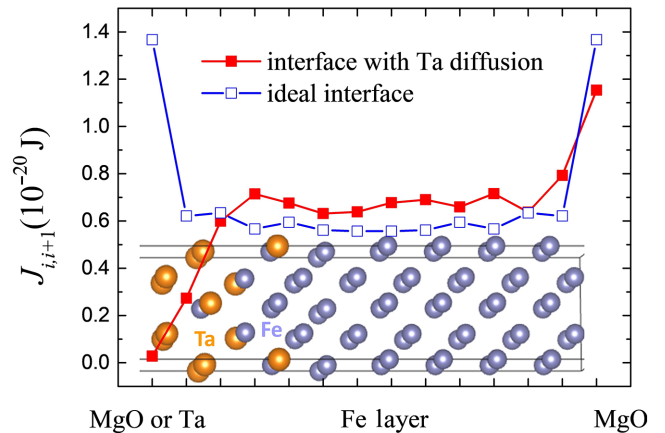


FIG. 7. The calculated nearest-neighbor-exchange constants across a 15-ML-thick Fe/MgO structure with Ta diffusion represented by solid red squares and compared to the values in an ideal Fe/MgO interface, represented by open blue squares. The inset displays the model structure used where the Ta atoms are introduced in the four outermost layers opposite to the MgO, with 100, 75, 50, and 25%, respectively.

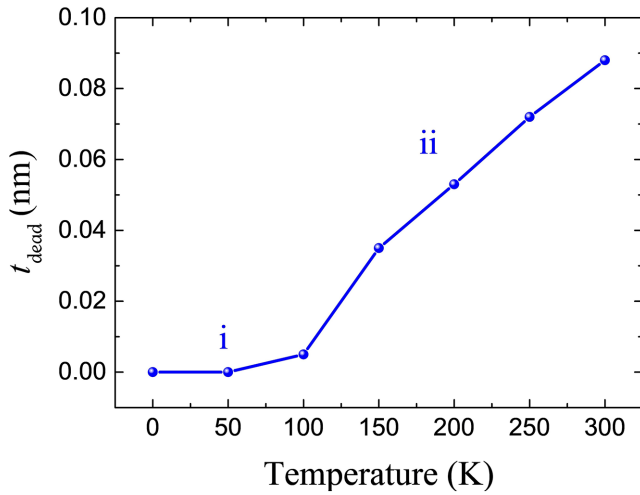


FIG. 8. The variation of the magnetic dead-layer thickness t_{dead} plotted as a function of temperature, showing two regimes: a negligible-thickness regime denoted by (i) and another revealing an increase of t_{dead} with temperature (ii).

In order to check how the magnetic dead layer affects the correlation between the temperature dependence of K and M_s , we calculate the scaling exponent as a function of the thickness of the system presented in Fig. 9, the variation of which can be fitted exponentially. Interestingly, the scaling exponent for all considered thicknesses deviates significantly from the Callen and Callen power law and lies in the range $1.5 \leq n \leq 2.2$. Thus, the low values of the experimental scaling exponents reported earlier can be attributed to the presence of a magnetic dead layer. Note that modeling magnetic dead layers in this way provides a qualitative insight into their influence on the temperature dependence of the magnetic properties of realistic samples. In other words, changing the model of the Ta diffusion

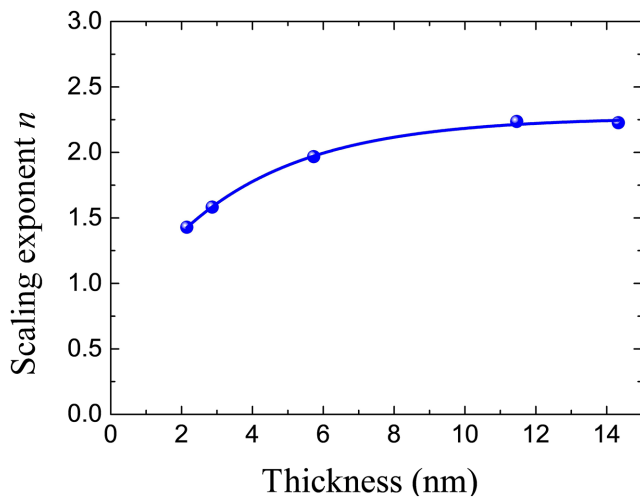


FIG. 9. The effect of the magnetic dead layer on the temperature dependence of K , revealed by the variation of the scaling exponent n as a function of the magnetic layer thickness.

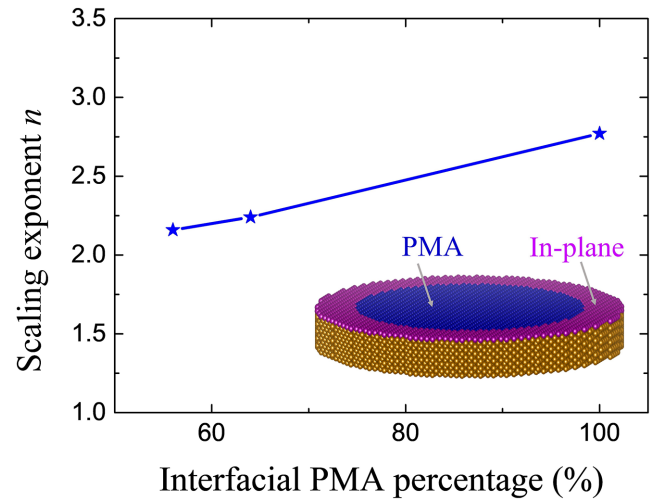


FIG. 10. The variation of the scaling exponent n , plotted as a function of the percentage of interfacial PMA obtained by employing the core-shell model shown in the inset.

would modify the exchange constants and, consequently, the values of the scaling exponents without changing the trend of its variation with the thickness of the sample.

VI. EFFECT OF INHOMOGENEITY IN PERPENDICULAR MAGNETIC ANISOTROPY

As already mentioned above, an analytical model [23,26] and recent experiments [24,28] have pointed out the presence of spatial fluctuations in the interfacial magnetic anisotropy. These fluctuations have been attributed to local variations in the ferromagnetic layer thickness associated with film roughness or to the diffusion of buffer-layer atoms through the ferromagnetic layer toward the MgO interface upon postdeposition annealing. Consequently, it is important to investigate the effect of inhomogeneous interfacial perpendicular magnetic anisotropy on its temperature dependence. We thus employ the core-shell model, comprising two regions at the interface, one with a perpendicular PMA and the other possessing in-plane magnetic anisotropy, the values of which are equal in magnitude but opposite in sign, as shown in the inset of Fig. 10. The resulting dependence of the scaling exponent on the percentage of the interfacial PMA is shown in Fig. 10. One can see that the scaling exponent decreases to values below 2.5 as the interfacial PMA percentage decreases. This highlights that the effect of interfacial roughness also plays a crucial role in the temperature dependence of the magnetic properties of MgO-based interfaces and leads to deviations from the theoretical Callen and Callen limit.

VII. CONCLUSIONS

The results presented in this work unveil several important mechanisms for understanding the temperature

dependence of the magnetic anisotropy at MgO-based interfaces. Based on small second-order anisotropy K_2 values obtained from first-principles calculations on ideally homogeneous interfaces, we conclude that the higher-order anisotropy terms observed in some experiments arise mainly from extrinsic contributions such as spatial fluctuations of first-order anisotropy. Therefore, only the first-order K_1 term is included in the atomistic spin Hamiltonian to describe the temperature dependence of the magnetic anisotropy. First-principles calculations of the layer-resolved exchange constants show an enhancement of the values at the Fe/MgO interface compared to the bulk, which provides a more accurate description of the temperature dependence of the magnetic properties in our atomistic model. In an ideal Fe/MgO interface, the temperature dependence of the total and layer-resolved anisotropy follow the Callen and Callen scaling power law and thus the intrinsic properties cannot explain deviations from this law. In this respect, we show that such deviations observed experimentally can be attributed to two macroscopic mechanisms: the presence of a magnetic dead layer and the spatial fluctuations of the interfacial PMA. In particular, the scaling exponent is found to vary with the thickness of the sample in the presence of a magnetic dead layer. In fact, this dependence has been observed in Ref. [35] at a Co/AlOx interface. It may be possible to distinguish between these two mechanisms experimentally in either of the following two ways: (i) thickness-dependent measurements can be performed in the knowledge that the mechanisms yield different thickness dependencies of n ; (ii) or interface-sensitive techniques such as Mössbauer experiments with an Fe-doped interfacial layer can give access to the interfacial magnetization. Accordingly, if scaling $K(T)$ by the interfacial magnetization only leads to $n = 3$ independent of the magnetic layer thickness, then a magnetic dead-layer mechanism can be concluded. Otherwise, still considering the interfacial magnetization only, the $n < 3$ scaling exponents indicate an inhomogeneous interfacial PMA mechanism. We anticipate that the provided description of the temperature dependence of the magnetic properties at MgO-based interfaces will be helpful for a fundamental and technical understanding of the thermal effects.

ACKNOWLEDGMENTS

We thank R. F. L. Evans for helpful discussions and acknowledge partial support by the Advanced Storage Research Consortium (ASRC) and by the European Research Council (ERC) Advanced Grant Project MAGICAL No. 669204.

APPENDIX A: CALCULATION METHODS

1. First-principles calculations

Our first-principles calculations are based on the projector-augmented-wave (PAW) method [36] as

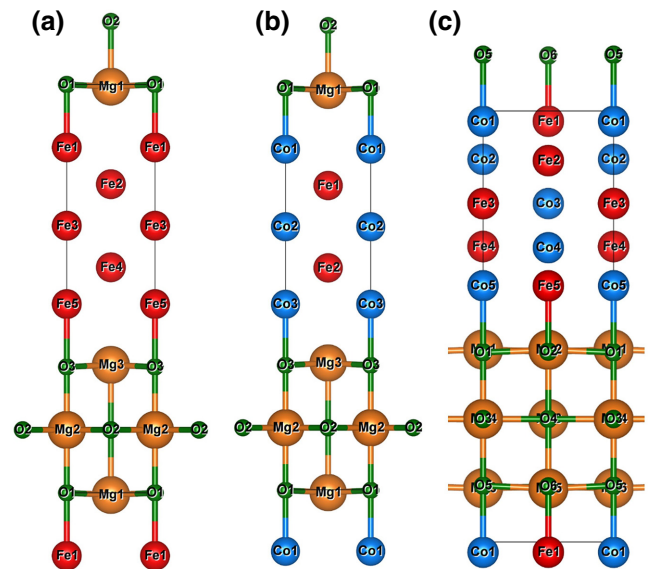


FIG. 11. The periodic structures used in the first-principles calculations: (a) Fe-, (b) Co-, and (c) Fe-Co-terminated MgO-based interfaces.

implemented in the VASP package [37–39] using the generalized gradient approximation [40] and including spin-orbit coupling within the second-order perturbation theory [41]. A kinetic energy cutoff of 550 eV is used for the plane-wave basis set and a $31 \times 31 \times 1$ k -point mesh to sample the first Brillouin zone. The periodic structures comprise five magnetic MLs, Fe or Fe-Co, sandwiched between five MLs of MgO, as shown in Fig. 11. As is known for the Fe/MgO interface, the most stable location for the oxygen atoms is on top of metal ions, due to the strong overlap between the Fe- $3d$ and O- $2p$ orbitals [13]. For the (Co-Fe)/MgO interface, Co-Fe has a Cs-Cl structure and it is in $B2$ -ordered phase, with the Co-Fe (100) parallel to the MgO (110) direction, where we consider two cases. The first is with Co termination, as shown in Fig. 11(b), which has been found to be the more stable in previous reports [42,43]. The second case is with 50% Fe-50% Co termination, as shown in Fig. 11(c), where the transition-metal atoms are located above the O atoms at the interface. All the structures are fully relaxed in atomic positions and volume until the forces become smaller than $1 \text{ meV}/\text{\AA}$. We find optimized lattice constants $a = 2.976, 2.918, \text{ and } 4.149 \text{ \AA}$ for the cases of Fe/MgO, Co-terminated (Fe-Co)/MgO, and Fe-Co-terminated (Fe-Co)/MgO, respectively. The layer-resolved magnetic anisotropy contributions are evaluated following Ref. [29].

The calculations of the exchange constants are done in two steps. First, first-principles calculations based on linear combination of atomic orbitals (LCAOs) are performed using the SIESTA package [44] within the Perdew-Burke-Ernzerhof (PBE) form of the exchange-correlation

functional [40]. A linear combination of numerical atomic orbitals with a double- ζ -polarized basis set, a real-space grid cutoff of 1000 Ry, and $25 \times 25 \times 3$ k -point sampling of the Brillouin zone are used. In the second step, the converged Hamiltonian and overlap matrix are used by the TB2J package [45] to calculate the long-range exchange interactions. This is done based on the Green's function method and using the magnetic force theorem, which takes the rigid spin rotation as a perturbation to the electronic structure. To perform atomistic calculations, the short-range exchange constants are obtained from the long-range ones by truncating to the nearest-neighbor interactions such that the exchange between an atom located at layer i and another at $i + 1$ is calculated by summing over all atomic planes above and below layer i , where $J_{i,i+1} = 1/4 \sum_{n \leq i, m > i} J_{n,m}$. Note that we perform additional tight-binding (TB)–linear-muffin-tin-orbital (LMTO) calculations [46] of the exchange interaction, which show similar trends with the Fe thickness.

2. Atomistic calculations

The atomistic calculations are based on the classical atomistic spin model implemented in the VAMPIRE package [33,47]. This allows us to study the influence of thermal spin fluctuations on the intrinsic magnetic properties such as the magnetization and magnetic anisotropy. The spin Hamiltonian including the exchange interaction and the uniaxial magnetic anisotropy is written as

$$H = - \sum_{i < j} J_{ij} \mathbf{S}_i \cdot \mathbf{S}_j - \sum_i k_u (\mathbf{S}_i \cdot \mathbf{e}_i)^2, \quad (\text{A1})$$

where J_{ij} is the isotropic exchange constant between nearest-neighbor atomic sites of local spin-moment directions \mathbf{S}_i and \mathbf{S}_j , k_u is the uniaxial anisotropy constant per atom, and \mathbf{e}_i is a unit vector along the magnetic easy axis. Only the first-order anisotropy constant is included in the Hamiltonian since our first-principles calculations demonstrate small second-order K_2 values. To model the Fe/MgO interface, we construct a cylindrical-shaped system with a 15-nm diameter and we vary the thickness t from the body-centered-cubic (bcc) Fe crystal of lattice parameter $a = 2.866 \text{ \AA}$. We fix the in-plane lattice parameter in all calculations, since we find that it has a negligible effect on the calculated properties (Appendix B). We divide the system into two regions: (i) bulk with negligible k_u and an atomic spin moment of $2.2 \mu_B$ and an (ii) interfacial region with an enhanced atomic spin moment of $2.76 (2.49) \mu_B$ and $k_u = 1.099 \times 10^{-22} (4.593 \times 10^{-23})$ J per atom for the first Fe1 (second Fe2) ML, respectively. Those site-resolved magnetic anisotropy values, shown in Fig. 12, are based on our first-principles calculations, revealing that the interfacial magnetic anisotropy in Fe/MgO is mainly contributed from the first and second Fe

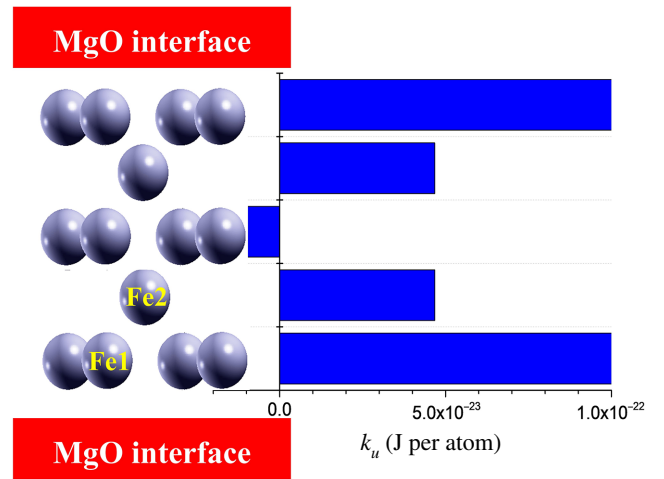


FIG. 12. The layer-resolved anisotropy energies to first order E_{MCA} at Fe/MgO interface, obtained from first-principles calculations, showing that both the first (Fe1) and second (Fe2) Fe MLs contribute to the PMA. Those values are used to parametrize the temperature-dependent atomistic calculations.

MLs [29]. The layer-resolved nearest-neighbor-exchange constants are obtained as described in Appendix A(1). The constrained Monte Carlo approach, as described in Ref. [48], is used to calculate the temperature-dependent saturation magnetization and the anisotropy of the modeled system. We use 100 000 Monte Carlo equilibration steps followed by 100 000 steps, with a 10^{-16} s time step, over which the thermodynamic averages are calculated to obtain the temperature-dependent properties of the system. We note that the calculated temperature-dependent magnetization and the anisotropy are normalized by their values at $T = 10$ K so as to be closer to experiments done at very low temperatures, where spin fluctuations are almost negligible.

APPENDIX B: CHOICE OF IN-PLANE LATTICE PARAMETER IN THE ATOMISTIC CALCULATIONS

As mentioned previously, our calculations are done in two steps. Our first-principles calculations start by optimizing the atomic structures through full relaxation of the atomic positions and the volume. In Fig. 13, we show the variation of the relaxed in-plane lattice parameter of Fe/MgO as a function of the Fe thickness. Here, one can clearly see how increasing the Fe thickness while keeping the MgO thickness fixed leads to a decrease in the lattice parameter getting closer to that of Fe $a = 2.866 \text{ \AA}$. Then, the calculated layer-resolved magnetic moments, magnetic anisotropy energies, and exchange interactions are obtained using those relaxed structures.

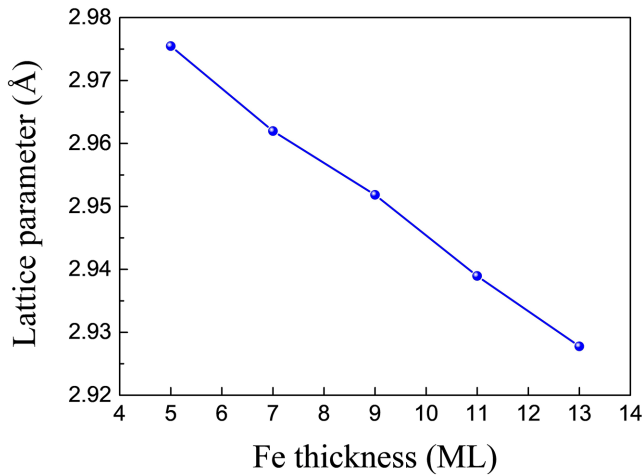


FIG. 13. The variation of the optimized in-plane lattice parameter of the Fe/MgO supercell with the Fe thickness.

The atomistic calculations are parametrized with the layer-resolved magnetic moments, anisotropy energies, and exchange interactions obtained from first principles using optimized structures. Namely, we fix the in-plane lattice parameter in the modeled cylindrical-shaped samples to $a = 2.866$ Å. In order to compare and verify that the effect of the lattice parameter is minor, we perform test calculations using the *ab initio* optimized lattice constants. For instance, the results of those two calculations for 11-ML-thick Fe samples are compared in Fig. 14. One can see that both the normalized saturation magnetization (M) and the magnetic anisotropy (K) dependencies as a function of temperature are hardly affected by the choice of the lattice parameter. Consequently, the scaling exponent of their temperature dependence, on which we focus in the present study, is also not affected.

APPENDIX C: LAYER-RESOLVED CHANGE OF THE MAGNETIZATION AS A FUNCTION OF TEMPERATURE

The decrease of the magnetization with temperature is indeed layer dependent. In case of an ideal interface, the layer-resolved saturation magnetization for the different layers is compared in Fig. 5(a). The magnetization of second iron layer (Fe2) decreases more slowly with temperature compared with that of the first (Fe1) and the bulk region. This can be explained by the enhanced exchange at the interface, namely in the nearest-neighbor pair interaction $J_{1,2}$ compared to the bulk values accompanied by reduced atomic coordination of the Fe1 layer and full coordination of Fe2.

In case of the presence of a dead layer, we show the layer-resolved variation of the normalized magnetization (M) as a function of temperature in Fig. 15. The previous explanation still holds for the upper interface, which is

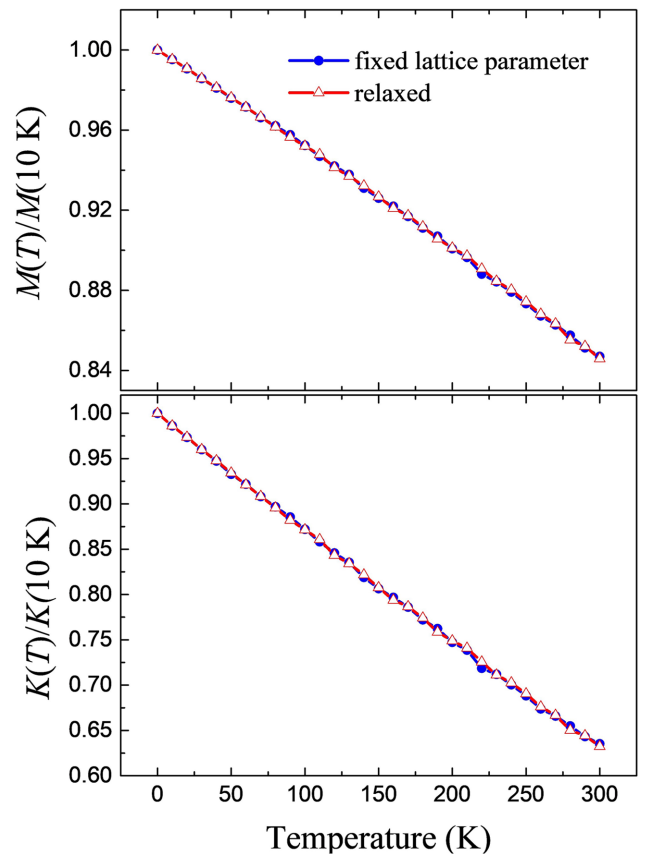


FIG. 14. The temperature dependence of the normalized magnetization and anisotropy obtained from the atomistic calculations using either the *ab initio* optimized lattice constant or fixed to that of Fe.

ideal, and we can observe an almost identical trend for all the bulk layers. However, a faster decrease of M is found for the lower interface. This is due to the reduced exchange caused by the Ta diffusion, namely in Fe13-Fe14-Fe15, that can also be depicted in Fig. 7.

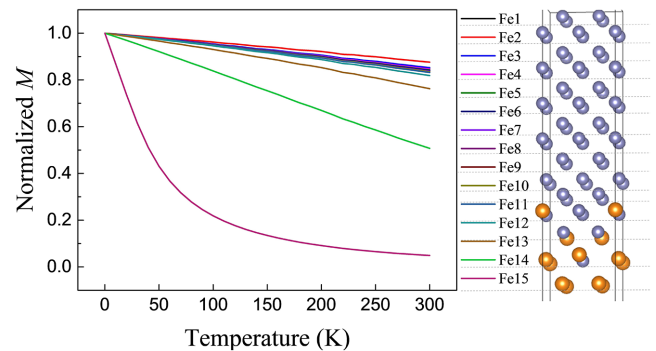


FIG. 15. The layer-resolved normalized magnetization as a function of temperature for a sample comprising a dead layer at its lower interface.

- [1] J. C. Slonczewski, Current-driven excitation of magnetic multilayers, *J. Magn. Magn. Mater.* **159**, L1 (1996).
- [2] L. Berger, Emission of spin waves by a magnetic multilayer traversed by a current, *Phys. Rev. B* **54**, 9353 (1996).
- [3] T. Kawahara, K. Ito, R. Takemura, and H. Ohno, Spin-transfer torque RAM technology: Review and prospect, *Microelectron. Reliab.* **52**, 613 (2012).
- [4] A. D. Kent and D. C. Worledge, A new spin on magnetic memories, *Nat. Nanotechnol.* **10**, 187 (2015).
- [5] D. Apalkov, B. Dieny, and J. Slaughter, Magnetoresistive random access memory, *Proc. IEEE, Inst. Electr. Electron. Eng.* **104**, 1796 (2016).
- [6] A. V. Khvalkovskiy, D. Apalkov, S. Watts, R. Chepulskii, R. S. Beach, A. Ong, X. Tang, A. Driskill-Smith, W. H. Butler, P. B. Visscher, D. Lottis, E. Chen, V. Nikitin, and M. Krounbi, Basic principles of STT-MRAM cell operation in memory arrays, *J. Phys. D: Appl. Phys.* **46**, 074001 (2013).
- [7] S. Ikeda, K. Miura, H. Yamamoto, K. Mizunuma, H. D. Gan, M. Endo, S. Kanai, J. Hayakawa, F. Matsukura, and H. Ohno, A perpendicular-anisotropy CoFeB-MgO magnetic tunnel junction, *Nat. Mater.* **9**, 721 (2010).
- [8] G. Jan, Y.-J. Wang, T. Moriyama, Y.-J. Lee, M. Lin, T. Zhong, R.-Y. Tong, T. Tornø, and P.-K. Wang, High spin torque efficiency of magnetic tunnel junctions with MgO/CoFeB/MgO free layer, *Appl. Phys. Express* **5**, 093008 (2012).
- [9] B. Dieny and M. Chshiev, Perpendicular magnetic anisotropy at transition metal/oxide interfaces and applications, *Rev. Mod. Phys.* **89**, 025008 (2017).
- [10] B. Rodmacq, S. Auffret, B. Dieny, S. Monso, and P. Boyer, Crossovers from in-plane to perpendicular anisotropy in magnetic tunnel junctions as a function of the barrier degree of oxidation, *J. Appl. Phys.* **93**, 7513 (2003).
- [11] A. Manchon, C. Ducruet, L. Lombard, S. Auffret, B. Rodmacq, B. Dieny, S. Pizzini, J. Vogel, V. Uhlir, M. Hochstrasser, and G. Panaccione, Analysis of oxygen induced anisotropy crossover in Pt/Co/MOx trilayers, *J. Appl. Phys.* **104**, 043914 (2008).
- [12] L. E. Nistor, B. Rodmacq, S. Auffret, and B. Dieny, Pt/Co/oxide and oxide/Co/Pt electrodes for perpendicular magnetic tunnel junctions, *Appl. Phys. Lett.* **94**, 012512 (2009).
- [13] H. X. Yang, M. Chshiev, B. Dieny, J. H. Lee, A. Manchon, and K. H. Shin, First-principles investigation of the very large perpendicular magnetic anisotropy at Fe—MgO and Co—MgO interfaces, *Phys. Rev. B* **84**, 054401 (2011).
- [14] S. Bandiera, R. C. Sousa, M. M. de Castro, C. Ducruet, C. Portemont, S. Auffret, L. Vila, I. L. Prejbeanu, B. Rodmacq, and B. Dieny, Spin transfer torque switching assisted by thermally induced anisotropy reorientation in perpendicular magnetic tunnel junctions, *Appl. Phys. Lett.* **99**, 202507 (2011).
- [15] E. R. Callen and H. B. Callen, Static magnetoelastic coupling in cubic crystals, *Phys. Rev.* **129**, 578 (1963).
- [16] E. R. Callen and H. B. Callen, The present status of the temperature dependence of magnetocrystalline anisotropy, and the $I(I + 1)/2$ power law, *J. Phys. Chem. Solids* **27**, 1271 (1966).
- [17] H. D. Gan, H. Sato, M. Yamanouchi, S. Ikeda, K. Miura, R. Koizumi, F. Matsukura, and H. Ohno, Origin of the collapse of tunnel magnetoresistance at high annealing temperature in CoFeB/MgO perpendicular magnetic tunnel junctions, *Appl. Phys. Lett.* **99**, 252507 (2011).
- [18] J. G. Alzate, P. K. Amiri, G. Yu, P. Upadhyaya, J. A. Katine, J. Langer, B. Ocker, I. N. Krivorotov, and K. L. Wang, Temperature dependence of the voltage-controlled perpendicular anisotropy in nanoscale MgO—CoFeB—Ta magnetic tunnel junctions, *Appl. Phys. Lett.* **104**, 112410 (2014).
- [19] H. Sato, P. Chureemart, F. Matsukura, R. W. Chantrell, H. Ohno, and R. F. L. Evans, Temperature-dependent properties of CoFeB/MgO thin films: Experiments versus simulations, *Phys. Rev. B* **98**, 214428 (2018).
- [20] O. N. Mryasov, U. Nowak, K. Y. Guslienko, and R. W. Chantrell, Temperature-dependent magnetic properties of FePt: Effective spin Hamiltonian model, *Europhys. Lett.* **69**, 805 (2005).
- [21] R. Skomski, O. N. Mryasov, J. Zhou, and D. J. Sellmyer, Finite-temperature anisotropy of magnetic alloys, *J. Appl. Phys.* **99**, 08E916 (2006).
- [22] L. Cuchet, B. Rodmacq, S. Auffret, R. C. Sousa, and B. Dieny, Influence of magnetic electrodes thicknesses on the transport properties of magnetic tunnel junctions with perpendicular anisotropy, *Appl. Phys. Lett.* **105**, 052408 (2014).
- [23] B. Dieny and A. Vedyayev, Crossover from easy-plane to perpendicular anisotropy in magnetic thin films: Canted anisotropy due to partial coverage or interfacial roughness, *Europhys. Lett.* **25**, 723 (1994).
- [24] A. A. Timopheev, R. Sousa, M. Chshiev, H. Nguyen, and B. Dieny, Second order anisotropy contribution in perpendicular magnetic tunnel junctions, *Sci. Rep.* **6**, 26877 (2016).
- [25] B. M. S. Teixeira, A. A. Timopheev, N. F. F. Caçoilo, S. Auffret, R. C. Sousa, B. Dieny, E. Alves, and N. A. Sobolev, Ion irradiation-induced easy-cone anisotropy in double-MgO free layers for perpendicular magnetic tunnel junctions, *Appl. Phys. Lett.* **112**, 202403 (2018).
- [26] B. Heinrich, T. Monchesky, and R. Urban, Role of interfaces in higher order angular terms of magnetic anisotropies: Ultrathin film structures, *J. Magn. Magn. Mater.* **236**, 339 (2001).
- [27] J. Z. Sun, Consequences of an interface-concentrated perpendicular magnetic anisotropy in ultrathin CoFeB films used in magnetic tunnel junctions, *Phys. Rev. B* **91**, 174429 (2015).
- [28] A. A. Timopheev, B. M. S. Teixeira, R. C. Sousa, S. Auffret, T. N. Nguyen, L. D. Buda-Prejbeanu, M. Chshiev, N. A. Sobolev, and B. Dieny, Inhomogeneous free layer in perpendicular magnetic tunnel junctions and its impact on the effective anisotropies and spin transfer torque switching efficiency, *Phys. Rev. B* **96**, 014412 (2017).
- [29] A. Hallal, H. X. Yang, B. Dieny, and M. Chshiev, Anatomy of perpendicular magnetic anisotropy in Fe/MgO magnetic tunnel junctions: First-principles insight, *Phys. Rev. B* **88**, 184423 (2013).
- [30] J. B. Mohammadi, K. Cole, T. Mewes, and C. K. A. Mewes, Inhomogeneous perpendicular magnetic anisotropy as a

- source of higher-order quasistatic and dynamic anisotropies, *Phys. Rev. B* **97**, 014434 (2018).
- [31] I. Turek, S. Blugel, G. Bihlmayer, and P. Weinberger, Exchange interactions at surfaces of Fe, Co, and Gd, *Czechoslovak J. Phys.* **53**, 81 (2003).
- [32] M. Milun, P. Pervan, and D. P. Woodruff, Quantum well structures in thin metal films: Simple model physics in reality?, *Rep. Prog. Phys.* **65**, 99 (2002).
- [33] R. F. L. Evans, W. J. Fan, P. Chureemart, T. A. Ostler, M. O. A. Ellis, and R. W. Chantrell, Atomistic spin model simulations of magnetic nanomaterials, *J. Phys. Condens. Matter* **26**, 103202 (2014).
- [34] Ta is chosen since it is widely used in experiments. We point out that the effect of the buffer layer is beyond the scope of the present study, which focuses on the mechanisms of the temperature dependence. However, it is an interesting issue that is worth addressing in the future.
- [35] S. Bandiera, Ph.D. thesis, Université Grenoble Alpes (2011).
- [36] P. E. Blöchl, Projector augmented-wave method, *Phys. Rev. B* **50**, 17953 (1994).
- [37] G. Kresse and J. Hafner, *Ab initio* molecular dynamics for liquid metals, *Phys. Rev. B* **47**, 558(R) (1993).
- [38] G. Kresse and J. Furthmüller, Efficient iterative schemes for *ab initio* total-energy calculations using a plane-wave basis set, *Phys. Rev. B* **54**, 11169 (1996).
- [39] G. Kresse and J. Furthmüller, Efficiency of *ab-initio* total energy calculations for metals and semiconductors using a plane-wave basis set, *Comput. Mater. Sci.* **6**, 15 (1996).
- [40] J. P. Perdew, K. Burke, and M. Ernzerhof, Generalized Gradient Approximation Made Simple, *Phys. Rev. Lett.* **77**, 3865 (1996).
- [41] G. van der Laan, Microscopic origin of magnetocrystalline anisotropy in transition metal thin films, *J. Phys.: Condens. Matter* **10**, 3239 (1998).
- [42] J. D. Burton, S. S. Jaswal, E. Y. Tsybal, O. N. Mryasov, and O. G. Heinonen, Atomic and electronic structure of the CoFeB/MgO interface from first principles, *Appl. Phys. Lett.* **89**, 142507 (2006).
- [43] K. H. Khoo, G. Wu, M. H. Jhon, M. Tran, F. Ernult, K. Eason, H. J. Choi, and C. K. Gan, First-principles study of perpendicular magnetic anisotropy in CoFe/MgO and CoFe/Mg₃B₂O₆ interfaces, *Phys. Rev. B* **87**, 174403 (2013).
- [44] J. M. Soler, E. Artacho, J. D. Gale, A. García, J. Junquera, P. Ordejón, and D. Sánchez-Portal, The SIESTA method for *ab initio* order-*n* materials simulation, *J. Phys.: Condens. Matter* **14**, 2745 (2002).
- [45] X. He, N. Helbig, M. J. Verstraete, and E. Bousquet, Tb2j: A PYTHON package for computing magnetic interaction parameters, *Comput. Phys. Commun.* **264**, 107938 (2021).
- [46] D. Pashov, S. Acharya, W. R. L. Lambrecht, J. Jackson, K. D. Belashchenko, A. Chantis, F. Jamet, and M. van Schilfgaarde, QUESTAAL: A package of electronic structure methods based on the linear muffin-tin orbital technique, *Comp. Phys. Comm.* **249**, 107065 (2020).
- [47] VAMPIRE software package, version 5, <http://vampire.york.ac.uk/>.
- [48] P. Asselin, R. F. L. Evans, J. Barker, R. W. Chantrell, R. Yanes, O. Chubykalo-Fesenko, D. Hinzke, and U. Nowak, Constrained Monte Carlo method and calculation of the temperature dependence of magnetic anisotropy, *Phys. Rev. B* **82**, 054415 (2010).